Title: Ab initio study of absorption resonance correlations between nanotubes and nanoribbons of graphene and hexagonal boron nitride.

Authors: Renebeth B. Payod[1,*] and Vasil A. Saroka[2,3, §]

[1]Physics Department, De La Salle University, 2401 Taft Avenue, 0922 Manila, Philippines

[2]Center for Quantum Spintronics, Department of Physics, Norwegian University of Science and Technology, NO-7491, Trondheim, Norway

[3]Institute for Nuclear Problems, Belarusian State University, 220030 Minsk, Belarus

*e-mail: renebeth.payod@dlsu.edu.ph

§email: vasil.saroka@ntnu.no

Abstract.

Density functional theory calculations are performed for the electronic band structures and optical absorption spectra of the zigzag nanoribbons and armchair nanotubes of graphene and hexagonal boron nitride as well as hybrid tubular structures obtained by embedding two dimer lines of B and N atoms into an armchair nanotube. Linear correlation coefficient analysis is carried out to quantitatively investigate relations between energies of absorption resonances in these tube-ribbon pairs. Despite the large disparity in the energy band gaps of some of these structures, our results show a high degree of correlation ($r > 0.85$ with > 95% confidence level) between them.

Key words: nanoribbons, nanotubes, optical absorption, density functional theory, Pearson correlation coefficient

1. INTRODUCTION

Graphene is known to be a promising optoelectronic material due to its strong interaction with light defined by the fine structure constant [1]. However, the optical absorption of graphene is constant for a wide spectral range [1] which would require bandstructure modifications for switchable optoelectronic devices [2-5]. Current advances to the synthesis of graphene nanoribbons (GNR) [6] and carbon nanotubes (CNT) [7-8] have mainly addressed the issues on the bandgap opening and optical resonance engineering for high-performance devices.

A two-dimensional (2D) hexagonal boron nitride (h-BN) is another current breakthrough in nanomaterials. With an atomic arrangement of alternating boron and nitrogen atoms, h-BN has a layered structure similar to graphene. However, unlike graphene, pristine h-BN possesses a band gap higher than 5 eV [9-11]. Nevertheless, in-gap states can be introduced into the h-BN membrane with h-BN properties being modified drastically [12-14]. The h-BN band structure can also be changed by the formation of stable nanotubes [15] or by electron confinement in h-BN nanoribbons and hybrid h-BN/carbon structures [16-17]. The unique properties of h-BN are being efficiently combined with graphene and practically harnessed through high-quality embedment of graphene nanostructures into the h-BN membrane [18-19].

Despite the recent growth of research to the energy band optimization on graphene and h-BN, integration of the said nanomaterials into optoelectronic circuits still remain a major common issue. The architecture of optoelectronic circuits plays an important role to their large scale on-chip integration and transfer from the planar solid-state technology (2D circuits) to 3D circuits [20]. Seamlessly combining the properties of tubular and planar topologies is one of the key aspects of circuit nanoengineering. Thus, mapping the optical properties of tubular structures such as CNT and h-BN nanotubes (h-BNNT) to their counterparts, like zigzag GNR

(ZGNR) and h-BN zigzag nanoribbons (h-BNZNR), is necessary for applications in scalable photonic technology and on-chip device integration.

Previous tight-binding studies have shown manifestations of hidden correlation on the absorption resonances between of graphene nanoribbons and their corresponding tubes [21-23]. Although the selection rules for the optical transitions in GNRs and CNTs are generally different, the absorption resonances can be aligned when the width of the nanoribbon is half to the circumference of the nanotube [21, 23-24].

In this work, correlation analysis is conducted for the absorption spectra obtained within the density functional theory not only for the graphene nanoribbons and carbon nanotubes forming a suitable geometric pair as stated above but also to the hexagonal boron nitride ribbons and tubes. Similar analysis is further carried out to hybrid graphene and hexagonal boron nitride nanotubes.

2. METHODS

For an infinitely long carbon nanotube (CNT), the tube structure is defined by two chiral indices (n,m) that were both set to 10. The CNT(10,10), which has been thoroughly studied both theoretically [25] and experimentally [26], is used as a reference in this study. Likewise, the infinitely long zigzag graphene nanoribbon (ZGNR) is set to width index w = 9 since ZGNR(9) and CNT(10,10) can form a "tube-ribbon" pair as predicted in previous studies [21,23]. Boron nitride tube-ribbon pairs are investigated by comparisons of h-BNNT(6,6) and h-BNNT(7,7) to h-BNZNR with w = 6 or to ZGNR(5). Similar to well-known stable nanostructures of h-BN/graphene [27-29], tubes recognized as hybrid h-BN/CNT with chiral indices set to 6 and its inverse hybrid nanotube are explored as suitable tube-ribbon pairs for ZGNR(5). The inverse hybrid h-BN/CNT(6,6) has one of its covalently bonded B-N pair at a 180° rotation from the structure of a hybrid h-BN/CNT(6,6).

The periodic translation is oriented along the *x*-axis for all the nanotubes considered in this study.

The electronic band structures of the above-mentioned nanostructures are calculated using Quantum Espresso (QE) package based on the density functional theory (DFT) [30]. Norm-conserving pseudopotentials [31] are used in this calculation with Perdew-Burke-Ernzerhof (PBE) exchange and correlations [32]. The vacuum distances used for the separation of periodic nanostructure images are summarized in Table 1. In all the QE calculations, the kinetic energy cutoff to the plane wave expansion is set to 360 Ry.

Table 1. The translation periods and vacuum separations for the periodic images of graphene and hexagonal boron nitride nanotubes and nanoribbons

Structure type		x-axis (Å)	y-axis (Å)	z-axis (Å)
Ribbon	**ZGNR(5)**	2.46	20.0	10.0
	ZGNR(9)	2.46	40.0	20.0
	h-BNZNR(6)	2.51	20.0	10.0
Tube	**CNT(10,10)**	2.46	40.0	20.0
	h-BNNT(6,6)	2.51	40.0	20.0
	h-BNNT(7,7)	2.51	20.0	20.0
	Hybrid h-BN/CNT(6,6)	2.51	20.0	20.0
	Inverse hybrid h-BN/CNT(6,6)	2.51	20.0	20.0

Uniform k-point meshes given by 300 x 1 x 1 and 180 x 1 x 1 are used for the graphene and h-BN nanostructures, respectively. The dielectric function ε is computed in pw2gw subpackage of QE [30]. The resulting optical absorption spectra $A(\omega)$ are evaluated using Eq. (1) from Ref. [33]. Only the absorption spectra of the polarization parallel to the longitudinal axis is considered since the absorption from the radiation at the perpendicular polarization is normally weak [33] or suppressed due to the depolarization effect [34].

The degree of correlation between a sample set of absorption peaks (x_i, y_i) from two nanostructures *X* (tube) and *Y* (ribbon) is tested by the Pearson linear correlation coefficient, *r* defined by [35]

$$r = \frac{\sum(x_i - \bar{x})(y_i - \bar{y})}{\sqrt{\sum(x_i - \bar{x})^2}\sqrt{\sum(y_i - \bar{y})^2}}\,. \quad (1)$$

The confidence level is estimated based on the critical values of *r* in Table A.24 reported by Bonamente [35].

3. RESULTS AND DISCUSSION

The electronic band structures for all possible nanostructure ribbon-tube pairs are condensed into the subgraphs of Fig. 1. Consequently, Fig. 2 illustrates the corresponding absorption spectra from the given nanoribbons and nanotubes. In Fig. 1(a), a Dirac point is observed close to the *k*-point $2\pi/3$ of the CNT(10,10) energy band spectrum which therefore implies negligible curvature effects for a metallic CNT [36-37]. The corresponding CNT(10,10) optical absorption in Fig. 2 reveals the first interband peak E_1 at 1.575 eV indicating that a transition between the lowest conduction band and highest valence band is indeed forbidden.

The linear correlation coefficient between the absorption peaks of CNT(10,10) and ZGNR(9) is calculated to be equal to 0.9740, which means that the two structures have a very high correlation of peaks with a confidence level > 95 %. Hence, the predicted hidden correlation between GNR and CNT associated to van Hove singularities from the tight-binding model [21, 23] persists in the DFT QE numerical calculations.

From this high degree of correlation between graphene nanotube and nanoribbons, a similar pattern is expected for h-BN tube-ribbon pairs. Based on the calculated absorption spectra in Fig. 2, the absorption peak correlation coefficients are computed for each pair of h-BN nanotube and h-BN (or graphene) nanoribbon. The coefficients are shown in Table 2 with their corresponding confidence level estimated from *N* sample set of resonance peaks.

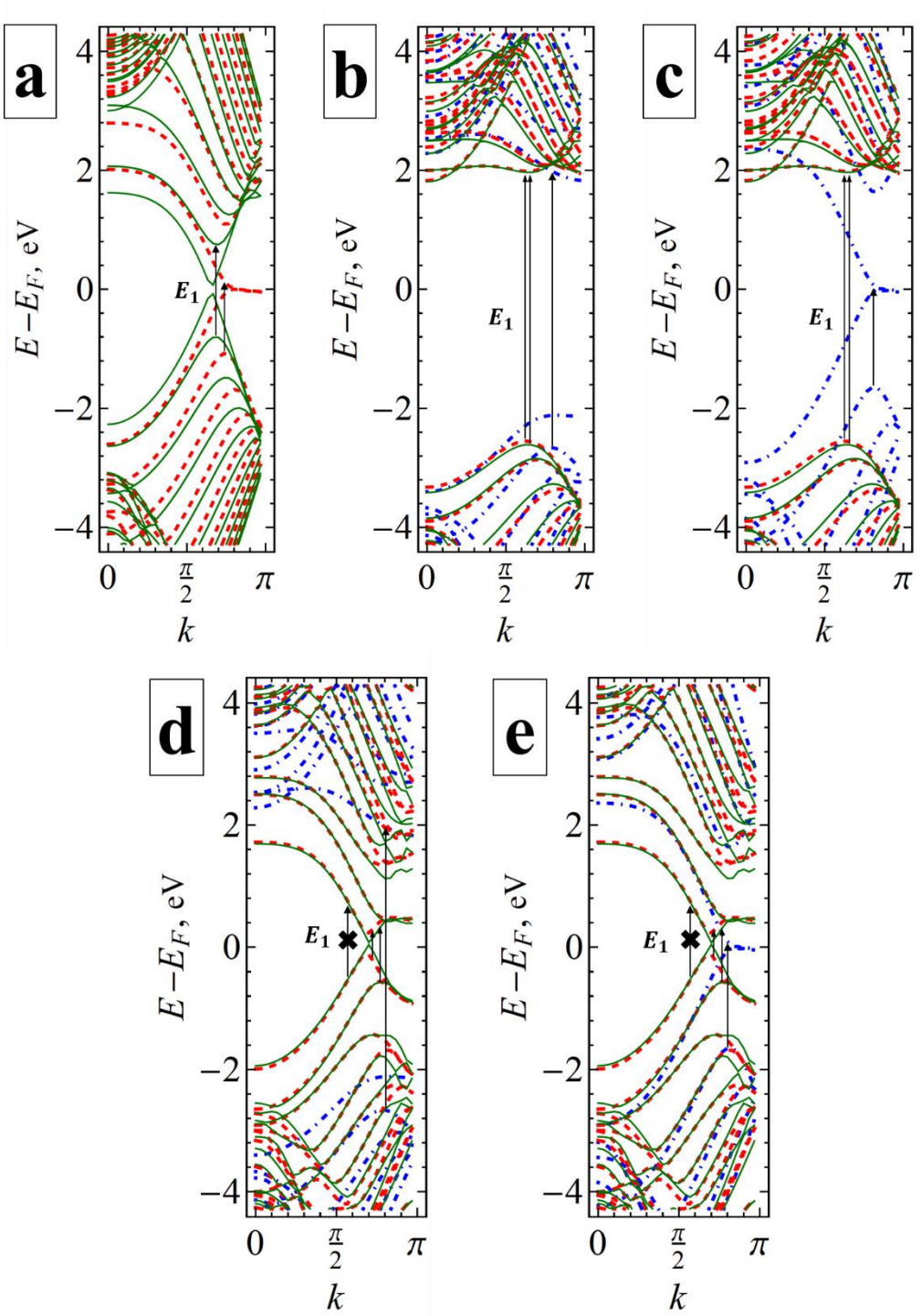

Fig. 1. The comparison between electronic band diagrams of **(a)** CNT(10,10) (solid green) and ZGNR(9) (dashed red), **(b)** h-BNNT(7,7) (solid green), h-BNNT(6,6) (dashed red) and h-BNZNR(6) (dashed dotted blue) **(c)** same as (b) but with dashed dotted blue curve being ZGNR(5), **(d)** inverse hybrid h-BN/CNT(6,6) (solid green),

hybrid h-BN/CNT(6,6) (dashed red) and h-BNZNR(6) (dashed dotted blue), **(e)** same as (d) but with dashed dotted blue curve being ZGNR(5). Black arrows denote allowed E_1 transitions while the crossed arrows are forbidden transitions.

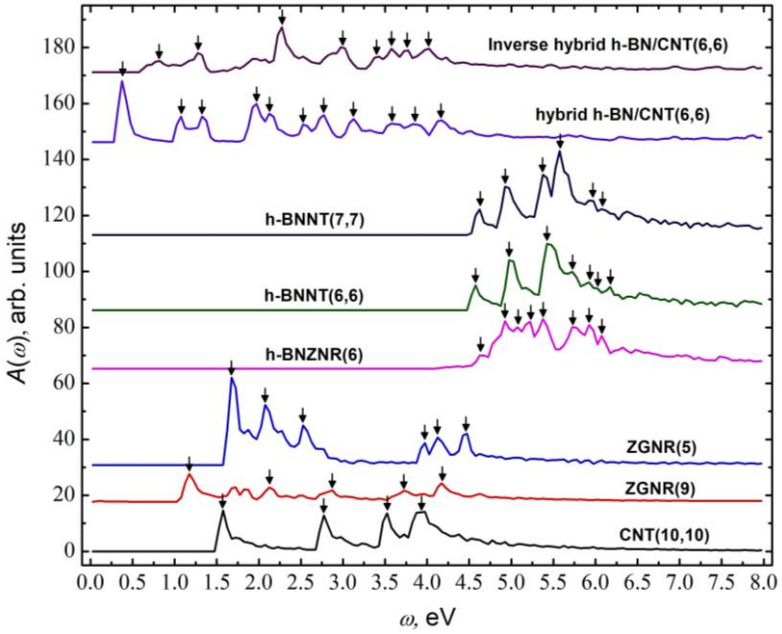

Fig. 2. The absorption spectra of the graphene and hexagonal boron nitride nanoribbons and nanotubes where the black arrows designate the resonance peaks.

Table 2. The Pearson correlation coefficient between the absorption peaks energies for different tube-ribbon pairs and the corresponding confidence level.

Nanoribbon	Nanotube	Correlation coefficient, *r*	Confidence level	Number of peaks, *N*
ZGNR(9)	CNT(10,10)	0.9740	95% - 99%	4
h-BNZNR(6)	h-BNNT(6,6)	0.6036	70% - 80%	6
h-BNZNR(6)	h-BNNT(7,7)	0.6020	70% - 80%	6
ZGNR(5)	h-BNNT(6,6)	0.9650	> 99%	6
ZGNR(5)	h-BNNT(7,7)	0.9589	> 99%	6
ZGNR(5)	hybrid h-BN/CNT(6,6)	0.4521	60% - 70%	6
ZGNR(5)	Inverse hybrid h-BN/CNT(6,6)	0.6474	80% - 90%	6
h-BNZNR(6)	hybrid h-BN/CNT(6,6)	0.6324	90% - 95%	8
h-BNZNR(6)	Inverse hybrid h-BN/CNT(6,6)	0.8748	> 99%	8

From the wide band gaps seen in Fig. 1(b), the first allowed high-energy interband transitions E_1 are located at 4.575 eV, 4.625 eV and 4.675 eV for h-BNNT(6,6)/h-BNNT(7,7) and h-BNZNR(6), respectively as shown in Fig. 2. These DFT QE

optical resonance results agree seamlessly to the DFT SIESTA numerical analysis done by Chernozatonskii et. al [28-29] which states that the band gap of a BN monolayer ($E_{BN\ mono} \approx 4.6$ eV) shortens as its energy branches approach the Fermi level due to the increase of the BN nanomesh curvature. However, the optical resonance correlations between a h-BNZNR(6) and the tubes h-BNNT(6,6) and h-BNNT(7,7) are not as high as the pairs of ZGNR(5) and these h-BNNTs. Despite a high degree of correlation between ZGNR(5) and the h-BNNTs, the absorption peaks are not aligned in ZGNR(5) and the h-BNNTs as shown in Fig. 2. For ZGNR(5), the interband transition E_1 is 1.675 eV while h-BNNTs have high-energy E_1 transitions. Based from these interesting results, correlation comparisons are then performed between hybrid h-BN/CNT and ribbons ZGNR and h-BNZNR. The electronic band diagrams in Fig. 1 (d) and (e) clearly show that the hybrid h-BN/CNT(6,6) exhibits semiconductor-to-metal transition upon its transformation into an inverse hybrid h-BN/CNT(6,6). With this change, the interband absorption peak $E_1 \approx 0.375$ eV of the hybrid h-BN/CNT(6,6) vanishes in the corresponding inverse hybrid tube, which clearly indicates that the interband dipole transition across the narrow band gap is indeed allowed for the hybrid structure. In contrast, the inverse hybrid h-BN/CNT(6,6) interband transition E_1 is 0.825 eV that evidently implies a forbidden dipole transitions in the vicinity of the Dirac point as shown by the crossed transition arrow in Fig. 1 (e). A similar behavior is also known for optical transitions across the narrow bandgaps induced by a magnetic field in armchair carbon nanotubes [24, 38] or by the curvature effects in quasi-metallic carbon nanotubes [37]. As specified in Table 2, the hybrid and inverse hybrid h-BN/CNT(6,6) correlation values are calculated to be less for ZGNR(5) compared to the high energy band gap h-BNZNR(6). Further scrutiny to the respective energy bands of h-BNZNR(6) indicates that the energy curves of h-BNZNR(6) do not have any direct resemblance to the hybrid h-BN/CNT(6,6) nor to

its inverse hybrid nanotube by which it gained the highest absorption correlation value. Therefore, more investigative tests and analysis are required to understand the high correlation between the pairs h-BNZNR and hybrid h-BN/CNT and its inverse hybrid nanotube.

4. CONCLUSIONS

In summary, high values of linear correlation were presented for the optical absorption resonances between tubular and ribbon nanostructure pairs of different compositions. In particular, high correlation coefficients ($r > 0.85$) were found for the following tube-ribbon pairs: ZGNR(9) and CNT(10,10), ZGNR(5) and h-BNNT(6,6), ZGNR(5) and h-BNNT(7,7), and h-BNZNR(6) and inverse hybrid h-BN/CNT(6,6). This significant degree of correlation, however, does not necessarily indicate alignment of the optical resonances as demonstrated by the ZGNR(5) and tubes h-BNNT(6,6) and h-BNNT(7,7). For the hybrid h-BN/CNT(6,6) structure, the band gap opening located at the Dirac point leads to distinct optical absorption transitions allowed across the gap.

ACKNOWLEDGMENTS

The authors are grateful to A.R. Villagracia for providing the computing workstation in STRC, De La Salle University – Manila, and to C.A. Downing, O. Pulci and D. Grassano for their helpful discussions.

FUNDING

V.A.S. acknowledges the financial support of EU H2020 RISE project CoExAN (Grant No. H2020-644076) and the RCN (Grant No. 274853), partly through its CoE funding scheme (Project No. 262633, “QuSpin”).

CONFLICT OF INTEREST

The authors declare no conflict of interest.

REFERENCES

1. R. R. Nair, P. Blake, A. N. Grigorenko, K. S. Novoselov, T. J. Booth, T. Stauber, N. M. R. Peres, and A. K. Geim, Science 320, 1308 (2008).
2. Q. Li, M. Liu, Y. Zhang, and Z. Liu, Small **12**, 1 (2016) pp. 32-50.
3. P. R. Wallace, Phys. Rev. **71**, 9 (1947) p. 622.
4. A.C. Neto, F. Guinea, N. M. Peres, K. S. Novoselov, and A. K. Geim, Rev. of Modern Phys., **81**, (2009) p.109.
5. K. S. Novoselov, S. V. Morozov, T. M. G. Mohinddin, L. A. Ponomarenko, D. C. Elias, R. Yang, I. I. Barbolina, P. Blake, T. J. Booth, D. Jiang, and J. Giesbers,. phys. status solidi (b) **244**, 11 (2007) pp. 4106-4111.
6. A. Celis, M. N. Nair, A. Taleb-Ibrahimi, E. H. Conrad, C. Berger, W. A. de Heer, and A. Tejeda, J. Phys. D. Appl. Phys. 49, 143001 (2016).
7. S. Zhang, L. Kang, X. Wang, L. Tong, L. Yang, Z. Wang, K. Qi, S. Deng, Q. Li, X. Bai, F. Ding, and J. Zhang, Nature (2017).
8. Q. Sun, R. Zhang, J. Qiu, R. Liu, and W. Xu, Adv. Mater. 30, 1705630 (2018).
9. K. Watanabe, T. Taniguchi, and H. Kanda, Nat. Materials **3**, 6 (2004) p. 404.
10. N. Alem, Q. M. Ramasse, C. R. Seabourne, O. V. Yazyev, K. Erickson, M. C. Sarahan, C. Kisielowski, A. J. Scott, S. G. Louie, and A. Zettl, Phys. Rev. Lett. **109**, 20 (2012) p. 205502.
11. A. Pakdel, Y. Bando, and D. Golberg, Chem. Soc. Rev. **43**, 3 (2014) pp.934-959.
12. Z. Liu, L. Ma, G. Shi, W. Zhou, Y. Gong, S. Lei, X. Yang, J. Zhang, J. Yu, K. P. Hackenberg, and A. Babakhani, Nat. Nanotechnol. **8**, 2 (2013) p. 119.
13. Z. Zhang, and W. Guo, Phys. Rev. B **77**, 7 (2008) p. 075403.
14. J. Wang, R. Zhao, Z. Liu, and Z. Liu, Small **9**, 8 (2013) pp. 1373-1378.
15. D. Golberg, Y. Bando, C. C. Tang, and C. Y. Zhi, Adv. Mater. 19, 2413 (2007).
16. C.-H. Park and S. G. Louie, Nano Lett. 8, 2200 (2008); F.-L. Shyu, Phys. B Condens. Matter 452, 7 (2014).
17. V.-T. Tran, J. Saint-Martin, and P. Dollfus, Appl. Phys. Lett. 105, 073114 (2014).
18. L. Chen, L. He, H. S. Wang, H. Wang, S. Tang, C. Cong, H. Xie, L. Li, H. Xia, T. Li, T. Wu, D. Zhang, L. Deng, T. Yu, X. Xie, and M. Jiang, Nat. Commun. 8, 14703 (2017).
19. D. Chen, R. Qiao, X. Xu, W. Dong, L. Wang, R. Ma, C. Liu, Z. Zhang, M. Wu, L. Liu, L. Bao, H.-T. Wang, P. Gao, K. Liu, and D. Yu, Nanoscale 11, 4226 (2019).

20. A. Todri-Sanial and C. S. Tan, *Physical Design for 3D Integrated Circuits* (CRC Press, Taylor and Francis Group, Florida, 2016).
21. V. A. Saroka, M. V. Shuba, amd M. E. Portnoi, Phy. Rev. B 95, 155438 (2017).
22. V. A. Saroka, K. G. Batrakov, V. A. Demin, and L. A. Chernozatonskii, J. Phys.: Condens. Matter 27, 145305 (2015)
23. V. A. Saroka, A. L. Pushkarchuk, S. A. Kuten, and M. E. Portnoi, J. of Saudi Chem. Soc. 22, 985 (2018).
24. M. E. Portnoi, V. A. Saroka, R. R. Hartmann, and O. V. Kibis, in 2015 IEEE Comput. Soc. Annu. Symp. VLSI (IEEE, 2015), pp. 456–459.
25. Deslippe, C. D. Spataru, D. Prendergast, and S. G. Louie, Nano Lett. 7, 1626 (2007).
26. K. Liu, J. Deslippe, F. Xiao, R. B. Capaz, X. Hong, S. Aloni, A. Zettl, W. Wang, X. Bai, S. G. Louie, E. Wang, and F. Wang, Nat. Nanotechnol. 7, 325 (2012).
27. L. A. Chernozatonskii, Y. K. Shimkus, and I. V. Stankevich, Phys. Lett. A 240, 105 (1998).
28. L. A. Chernozatonskii, V. A. Demin and A. A. Artyukh, JTEP Lett. 104, 1 (2016) pp. 43-48.
29. L. A. Chernozatonskii, V. A. Demin, S. Bellucci, Sci. Rep. 6, 38029 (2016).
30. P. Giannozzi, O. Andreussi, T. Brumme, O. Bunau, M. Buongiorno Nardelli, M. Calra, R. Car, C. Cavazzoni, D. Ceresoli, M. Cococcioni, N. Colonna, I. Carnimeo, A. Dal Corso, S. de Gironcoli, P. Delugas, et. al., J. Phys.: Condens. Matter 29, 465901 (2017).
31. D. R. Hamann, M. Schlüter, and C. Chiang, Phys. Rev. Lett. 43, 1494 (1979).
32. J. P. Perdew, K. Burke, and M. Ernzerhof, Phys. Rev. Lett. 77, 3865 (1996).
33. V. A. Saroka, H. Abdelsalam, V. A. Demin, D. Grassano, S. A. Kuten, A. L. Pushkarchuk, and O. Pulci, Semiconductors 52, 1890 (2018).
34. H. Ajiki and T. Ando, Phys. B: Condens. Matter 201, 349 (1994).
35. M. Bonamente, Statistics and Analysis of Scientific Data (Springer Science+Business Media, New York, 2013) pp. 154-156 & pp. 252-253.
36. E. B. Barros, A. Jorio, G. G. Samsonidze, R. B. Capaz, A. G. Souza Filho, J. Mendes Filho, G. Dresselhaus, M. S. Dresselhausm, Phys. Rep. 431, 261 (2006).
37. R. R. Hartmann, V. A. Saroka, and M. E. Portnoi, J. Appl. Phys. 125, 151607 (2019).
38. M. E. Portnoi, M. Rosenau da Costa, O. V. Kibis, and I. A. Shelykh, Int. J. Mod. Phys. B **23**, 2846 (2009)